Supporting Information

Lazarus and Constantine 10.1073/pnas.1214074110

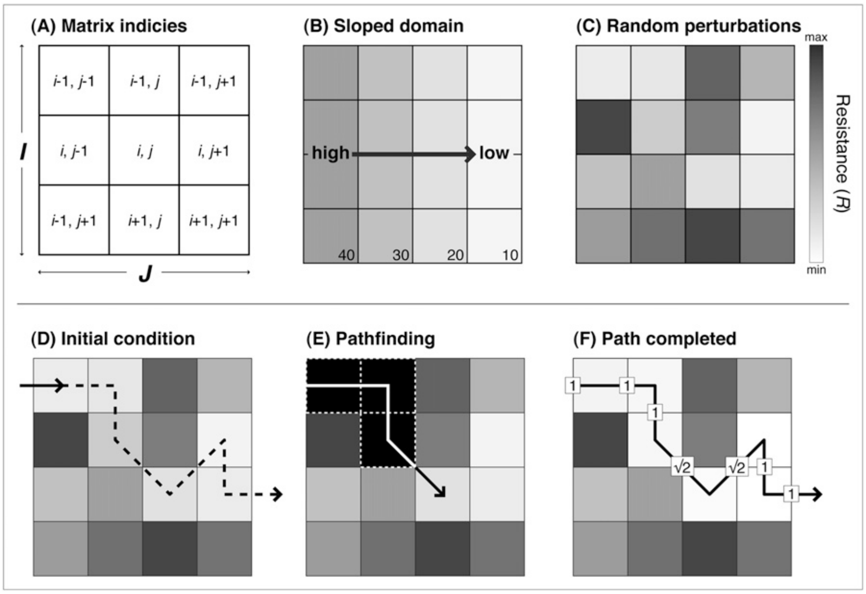

Fig. S1. Schematic of operations in our numerical flow-routing model. (*A*) Matrix indices relative to the center grid cell. (*B*) The parameter *S* determines the slope of the domain, from which (*C*) random values 0–*R* are subtracted. (*D*) From a given cell, the flow path moves to occupy whichever of its nearest neighbors has the lowest value. (*E*) As the flow path is developing, values of cells that the flow has occupied are temporarily reset to the unperturbed elevation at that cell, as in *B*. This value constitutes a local maximum that discourages the flow path from getting arbitrarily trapped by a local minimum, but does not necessarily prevent the path from recrossing itself, particularly when $R >> S$. (*F*) Once completed, cells occupied by the flow path are reset equal to the domain elevation given by *B*, minus the maximum perturbation *R*. Sinuosity is the total length of the flow path (arrows show the respective lengths of straight and diagonal steps) divided by the length dimension of the domain. The flow path in the schematic above, excluding the steps into and out of the grid, has sinuosity $\Omega = 5.82 \div 4 = 1.5$.

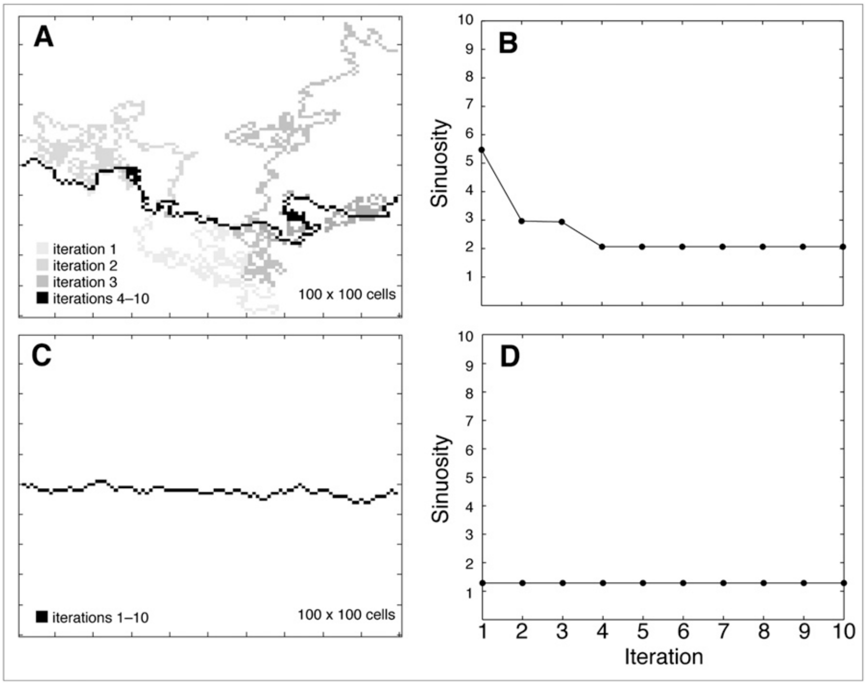

Fig. S2. Theoretically, sinuosity has no upper bound. However, where channel migration occurs in natural systems, flow dynamics tend to not only create excursive meanders but also cut them off, episodically shortening the overall channel length and reducing sinuosity. In the absence of a cutoff mechanism, resistance-dominated conditions ($R/S >> 1$) in our model will produce supersinuous patterns that are more numerical artifacts than useful analogs, a problem others have also encountered. We affect a cutoff-like function by updating and iterating the domain to allow the flow path to find a minimum length for a given combination of *R* and *S* that excludes numerical artifacts of supersinuous paths from the compiled results, particularly when $R >> S$. (*A*) Example of iterated flow paths and (*B*) corresponding sinuosities for $R = 0.04$ and $S = 0.001$. *C* and *D* show the comparatively locked planform of a slope-dominated, low-sinuosity channel ($R = 0.001$ and $S = 0.04$).

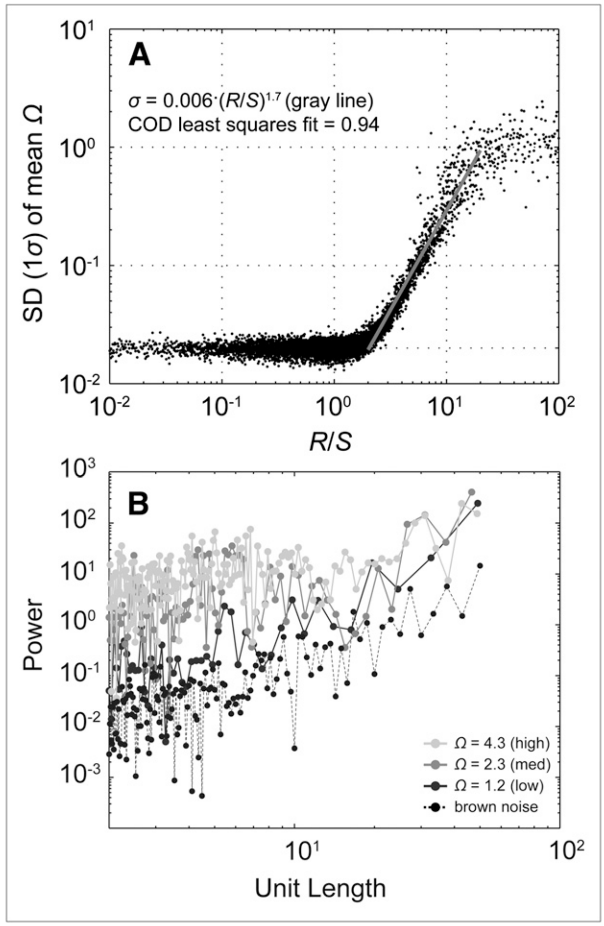

Fig. S3. (*A*) SD versus *R/S* of ensemble model runs. Variance scales with mean *R/S*. (*B*) Power spectra of representative modeled low-, medium-, and high-sinuosity planforms, with the power spectrum for a brown-noise signal (integral of a white-noise signal) for comparison. The model does not produce planforms with a preferred wavelength. Both *A* and *B* are indicative of the model's fundamentally Brownian structure.

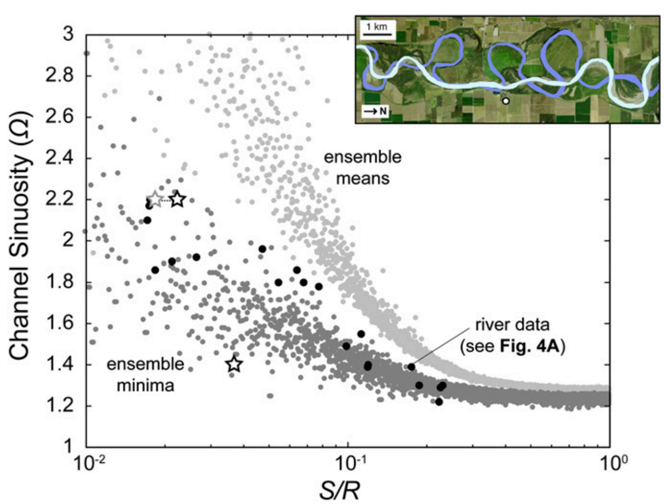

Fig. S4. Historical changes in the Sacramento River planform in terms of floodplain Froude number, plotted atop the data in Fig. 4*B*. The linked gray and black star symbols at $\Omega = 2.2$ mark the difference between assuming Manning's $n = 0.15$ (gray) or $n = 0.10$ (black) for the natural floodplain before 1874. Star symbol at $\Omega = 1.4$ reflects the effect of orchard plantations (here, $n = 0.05$) after 1898.

Table S1. Locations and credits for images shown in Figs. 1, 3, and 5

Fig.	Location	Source
1*A*	37.84°N, 126.21°E	(1)
1*B*	38.22°N, 109.88°W	(2)
1*C*	44.57°N, 70.71°W	(1)
1*D*	19.17°S, 35.08°W	(3)
1*E*	Mars: −6.008° (centered), 153.833°E	(4) location at center of image
1*F*	N/A	(5)
3*A*	51.51°N, 3.05°W	(1)
3*C*	56.42°N, 3.12°W	(1)
3*E*	51.36°N, 3.70°W	(1)
4*A*	64.43°N, 149.36°W	(1)
4*B*	64.49°N, 148.31°W	(1)
4*C*	39.46°N, 121.99°W	Digitized channels based on maps in ref. 6; base image 1

1. Google Inc. (2013) Google Earth (version 7.0.3.8542) [Software]. Available at www.google.com/earth/index.html. Accessed April 10, 2013.
2. National Agricultural Imagery Program (2006) Utah (natural color imagery), Tile q3335_ne_NAIP2006, NAIP Interactive Map. Available at http://mapserv.utah.gov/rasterindicies/naip2006.html. Accessed May 2012.
3. Gamboa D, Alves TM, Cartwright J (2012) A submarine channel confluence classification for topographically confined slopes. *Mar Pet Geol* 35(1):176–189.
4. High Resolution Imaging Science Experiment (2012) Yardangs and ridges of the edge of Aeolis Planum, Image PSP_006683_1740 (grayscale, map-projected), courtesy of NASA/JPL/University of Arizona. Available at www.uahirise.org/PSP_006683_1740. Accessed May 2012.
5. Lunar Reconnaissance Orbiter Mission (2012) NASA LROC WAC mosaic, courtesy of NASA/JPL/University of Arizona. Available at www.nasa.gov/images/content/503670main_120210a.jpg. Accessed May 2012.
6. Sullivan DG (1982) Prehistoric flooding in the Sacramento Valley: Stratigraphic evidence from Little Packer Lake, Glenn County, California. MS thesis (Univ of California, Berkeley, CA).

Table S2. Twenty meandering river reaches used in floodplain Froude number calculations

River name	Location	Valley slope ($\times 10^{-3}$)	Sinuosity	Floodplain Manning's *n*	Coordinates
Severn	United Kingdom	4.9 (1)	1.22*	0.10	52.74°N, 2.81°W
Jiu	Romania	5.0 (2)	1.29 (3)	0.10	44.17°N, 23.83°E
Republican	Nebraska	0.9 (4)	1.30 (4)	0.05	39.39°N, 97.18°W
Calamus	Nebraska	1.3 (5)	1.30 (5)	0.05	42.02°N, 99.47°W
Sacramento	California	0.8 (6)	1.39 (3)	0.05	39.44°N, 122°W
Peace	Canada	0.3 (7)	1.39 (3)	0.05	58.4°N, 114.75°W
Yampa	Colorado	0.2 (8)	1.40*	0.10	40.5°N, 107.5°W
Yellow	China	0.2 (9)	1.48 (3)	0.05	40.47°N, 109.35°E
Vyatka	Russia	0.3 (10)	1.55 (3)	0.05	58.38°N, 48.7°E
Liard	Canada	0.6 (11)	1.78 (3)	0.10	60.03°N, 128.88°W
Smoky Hill	Kansas	0.7 (4)	1.80 (4)	0.15	38.96°N, 96.91°W
Tana	Kenya	0.5 (12)	1.80 (3)	0.10	1.65°S, 40.11°E
Okavango	Botswana	0.4 (4)	1.86 (4)	0.10	18.10°W, 21.62°E
Ucayali	Peru	0.07 (13)	1.86 (3)	0.15	6.05°S, 74.85°W
Manu	Peru	0.1 (14)	1.90 (3)	0.15	12.7°S, 69.7°W
Beni	Bolivia	0.1 (15)	1.92 (3)	0.15	11.73°S, 66.78°W
Ramu	Papua New Guinea	0.5 (16)	1.96 (3)	0.15	4.13°S, 144.68°E
Jutai	Brazil	0.7 (17)	2.10 (3)	0.15	4.35°S, 67.9°W
Jurua	Brazil	0.7 (17)	2.17 (3)	0.15	4.45°S, 66.65°W
Purus	Brazil	0.7 (17)	2.20 (3)	0.15	6.88°S, 64.63°W

*Measured.

1. Carling PA, Orr HG (2000) Morphology of riffle-pool sequences in the River Severn, England. *Earth Surf Process Landforms* 25(4):369–384.
2. Radoane M, Radoane N, Dumitriu D (2003) Geomorphological evolution of longitudinal river profiles in the Carpathians. *Geomorphology* 50(4):293–306.
3. Constantine JA, Dunne T (2008) Meander cutoff and the controls on the production of oxbow lakes. *Geology* 36(1):23–26.
4. Vandenberg JH (1995) Prediction of alluvial channel pattern of perennial rivers. *Geomorphology* 12(4):259–279.
5. Bridge JS, Smith ND, Trent F, Gabel SL, Bernstein P (1986) Sedimentology and morphology of a low-sinuosity river – Calamus River, Nebraska Sand Hills. *Sedimentology* 33(6):851–870.
6. Constantine JA, Dunne T, Piegay H, Kondolf GM (2010) Controls on the alluviation of oxbow lakes by bed-material load along the Sacramento River, California. *Sedimentology* 57(2):389–407.
7. Hicks FE (1996) Hydraulic flood routing with minimal channel data: Peace River, Canada. *Can J Civ Eng* 23(2):524–535.
8. Merritt DM, Cooper DJ (2000) Riparian vegetation and channel change in response to river regulation: A comparative study of regulated and unregulated streams in the Green River Basin, USA. *Regul Rivers Res Manage* 16:543–564.
9. Xu JX (2002) River sedimentation and channel adjustment of the lower Yellow River as influenced by low discharges and seasonal channel dry-ups. *Geomorphology* 43(1-2):151–164.
10. Rysin I, Petukhova L (2004) Monitoring of channel processes on the interfluve between the Karma and the Vyatka rivers. *Sediment Transfer through the Fluvial System* (IAHS Press, Wallingford, UK) International Association of Hydrological Sciences Publication 288, p 261–268.
11. Quinton WL, Hayashi M, Pietroniro A (2003) Connectivity and storage functions of channel fens and flat bogs in northern basins. *Hydrol Processes* 17(18):3665–3684.
12. Veldkamp A, et al. (2007) Late Cenozoic fluvial dynamics of the River Tana, Kenya, an uplift dominated record. *Quat Sci Rev* 26(22-24):2897–2912.
13. Ettmer B, Alvarado-Ancieta CA (2010) Morphological development of the Ucayali River, Peru, without human impacts. *Ökosystemrenaturierung und nachhaltiges Management* 10:77–84.
14. Puhakka M, Kalliola R, Rajasilta M, Salo J (1992) River types, site evolution and successional vegetation patterns in Peruvian Amazonia. *J Biogeogr* 19(6):651–665.

15. Bourrel L, et al. (2007) Correlation between river slope and meandering variability (obtained by DGPS data) and morphotectonics for two Andean tributaries of the Amazon river: The case of Beni (Bolivia) and Napo (Ecuador-Peru) rivers. *AGU Spring Meeting Abstracts* H31D–02, 1:2.
16. Chappell J (1993) Contrasting Holocene sedimentary geologies of Lower Daly River, Northern Australia, and Lower Sepik-Ramu, Papua New Guinea. *Sediment Geol* 83(3-4):339–358.
17. Hendricks GA, et al. (2003) Channel slope from SRTM water surface elevations in the Amazon Basin. *AGU Fall Meeting Abstracts* H12D–1016, 1:1016.